5222 *Chem. Mater.* **2009,** *21,* 5222–5228
DOI:10.1021/cm902114d

CHEMISTRY OF MATERIALS
Article

Engineering Magnetic Properties of Ni Nanoparticles by Non-Magnetic Cores

HaiTao Zhang,* Jun Ding, GanMoog Chow, Min Ran, and JiaBao Yi

Department of Materials Science and Engineering, Faculty of Engineering, National University of Singapore, Singapore 117574

Received July 13, 2009. Revised Manuscript Received September 20, 2009

This work focuses on the magnetism-control study of nickel (Ni) nanoparticles (NPs) with non-magnetic cores of noble metals (M = Ag, Au). Monodispersed M NPs used as templates were synthesized by reducing their salt with a weak reductant—oleylamine (OA). The OA acted as surfactant and non-coordinating reagent in the preparation of Ni NPs with a narrow size distribution. Then Ni atoms were controlled to grow upon the M NPs by controlling the decomposition of nickel acetylacetonate in OA. The as-prepared M and core/shell M/Ni NPs exhibit spherical shape, as characterized by transmission electron microscopy. The systematic study indicated that the Ni shell exhibits face-centered cubic crystal structure and is relatively stable in air. The hydrophobic OA molecules on the surface could be exchanged by hydrophilic imidazole to make the samples water-soluble. Magnetic study of core/shell NPs indicated that their blocking temperatures could be tuned by modulating either core size or shell thickness. The novel magnetic properties of the core/shell structured NPs are introduced by the size effect, exchange interaction, and reduced magnetic ordering. The novel core/shell M/Ni NPs are expected to have a significant potential for biomolecule separation, magnetic imaging, and optoelectronics.

Introduction

Magnetic nanostructures have attracted much attention recently owing to their promising applications, such as magnetic resonance imaging (MRI) contrast enhancement, multi-terabit magnetic storage devices, conducting paints, rechargeable batteries, magnetic refrigeration systems, magnetic drug delivery, hyperthermia, magnetofection, optoelectronics, and magnetic biomolecules separation.[1] It should be noted that magnetic NPs prepared by different routes usually exhibit different (sometimes anomalous and paradox) physical properties. Therefore, exploring the intrinsic factors that affect the physicochemical properties of magnetic NPs is the prerequisite for designing nanostructures with expected/controllable properties. To cater to the diversified requirements for fundamental research and commercial applications, magnetic NPs with controllable size and shape have been fabricated widely by chemical and physical methods.[2] Extensive studies indicated that the colloidal chemical method is a prominent route to nanomaterials because of its capability of controlling physical and chemical properties. It can not only be used to synthesize single-component NPs but also be capable of fabricating multi-component hybrid NPs. These multi-component hybrid NPs generally exhibit promising synergistic functions, such as optical/magnetic properties and optical/catalytic properties.[3]

Ni, one of the most important ferromagnetic transition metals, exhibits a Curie temperature well above room temperature (631 K) and is being used in many fields, such as in hydrogen storage and ferrofluid.[1,4] To obtain high-quality Ni NPs, sonochemical or thermal decomposition of organometallic precursors in organic solvents,[5] chemical reduction,[6] electrochemical reduction,[7]

*Corresponding author. E-mail: zhanght@ustc.edu.

(1) (a) Gupta, A. K.; Gupta, M. *Biomaterials* **2005**, *26*, 3995. (b) Schmid, G. *Nanoparticles: From Theory to Applications*; Wiley-VCH: Weinheim, 2004. (c) O'Handley, R. C. *Modern Magnetic Materials: Principles and Application*; Wiley: New York, 2000. (d) Hironari, S.; Nakano, Y.; Matsushita, H.; Onoe, A.; Kanai, H.; Yamashita, Y. *J. Mater. Synth. Process.* **1998**, *6*, 415. (e) Antolini, E.; Ferretti, M.; Gemme, S. *J. Mater. Sci.* **1996**, *31*, 2187. (f) Gates, B. C. *Chem. Rev.* **1995**, *95*, 511. (g) Beecroft, L. L.; Ober, C. K. *Chem. Mater.* **1997**, *9*, 1302.

(2) (a) Murray, C. B.; Sun, S. H.; Doyle, H.; Betley, T. *MRS Bull.* **2001**, 985. (b) Puntes, V. F.; Krishnan, K. M.; Alivisatos, A. P. *Science* **2001**, *291*, 2115. (c) Chakka, V. M.; Altuncevahir, B.; Jin, Z. Q.; Li, Y.; Liu, J. P. *J. Appl. Phys.* **2006**, *99*, 08E912.

(3) (a) Cozzoli, P. D.; Pellegrino, T.; Manna, L. *Chem. Soc. Rev.* **2006**, *35*, 1195. (b) Shevchenko, E. V.; Talapin, D. V.; Kotov, N. A.; O'Brien, S.; Murray, C. B. *Nature* **2006**, *439*, 55. (c) Perepichka, D. F.; Rosei, F. *Angew. Chem., Int. Ed.* **2007**, *46*, 6006. (d) Zhang, H. T.; Ding, J.; Chow, G. M.; Dong, Z. L. *Langmuir* **2008**, *24*, 13197.

(4) Sakai, T.; Ishikawa, H.; Oguro, K.; Iwakura, C.; Yoneyam, H. *J. Electrochem. Soc.* **1987**, *3*, 558.

(5) (a) Koltypin, Y.; Fernández, A.; Rojas, T. C.; Campora, J.; Palma, P.; Prozow, R.; Gedanke, A. *Chem. Mater.* **1999**, *11*, 1331. (b) Caro, de D.; Bradley, J. S. *Langmuir* **1997**, *13*, 3067. (c) Park, J.; Kang, E.; Son, S. U.; Park, H. M.; Lee, M. K.; Kim, J.; Kim, K. W.; Noh, H. J.; Park, J. H.; Bae, C. J.; Park, J. G.; Hyeon, T. *Adv. Mater.* **2005**, *17*, 429. (d) Zhang, H. T.; Wu, G.; Chen, X. H.; Qiu, X. G. *Mater. Res. Bull.* **2006**, *41*, 495. (e) Winnischofer, H.; Rocha, T. C. R.; Nunes, W. C.; Socolovsky, L. M.; Hnobel, M.; Zanchet, D. *ACS Nano* **2008**, *2*, 1313.

(6) Hou, Y.; Kondoh, H.; Ohta, T.; Gao, S. *Appl. Surf. Sci.* **2005**, *241*, 218.

(7) (a) Cordente, N.; Amiens, C.; Chaudret, B.; Respaud, M.; Senocq, F.; Casanove, M. J. *J. Appl. Phys.* **2003**, *94*, 6358. (b) Ely, T. O.; Amiens, C.; Chaudret, B.; Snoeck, E.; Verelst, M.; Respaud, M.; Broto, J. M. *Chem. Mater.* **1999**, *11*, 526.

Published on Web 10/14/2009

and microwave-assisted polyol routes have been employed up to now.[8] Ni NPs have been proved to be applicable in biomolecule separations by recent study and are commercially available now.[9] A point that should be clarified is that Ni NPs, similar to soluble nickel, result in some toxicity to biomolecules/cells in some case.[9] However, the toxicity could be reduced to the satisfactory level through coating and formulation. Compared to metallic cobalt and iron NPs, Ni NPs are relatively stable in air owing to their better anticorrosion ability. The antioxidation ability of metallic Ni NPs decreases with decreasing particles size. Ni NPs tend to be totally oxidized by oxygen under air exposure when their size is below 5 nm.[5c] On the other hand, Ni NPs are generally expected to be small (to be superparamagnetic) in many applications, such as biomolecule separations and MRI.[9] To overcome this disadvantage, relatively bigger but still superparamagnetic Ni NPs are greatly welcome. However, the bigger NPs (size > 20 nm) are mostly not superparamagnetic at room temperature due to enhanced magnetic anisotropy energy and bigger volume.[10] Therefore, the fabrication method of superparamagnetic bigger Ni NPs is a technical challenge.

In this paper, we demonstrate a novel method to enlarge the overall particle size through non-magnetic core and keep the overall magnetic NPs superparamagnetic. Detailed microstructures and magnetic characterizations are presented.

Experimental Section

Synthesis of Ag NPs. Ag NPs were synthesized by using the procedure reported by Chen et al.[11] Typically, 0.5 g of $AgNO_3$, 8 mL of OA, and 40 mL of paraffin oil were added into a three-neck round-bottom flask equipped with a condenser, a thermocontroller, and a magnetic stirring bar. Then the mixture was stirred at 40 °C overnight under flowing N_2 gas, annealed at 180 °C for 2 h, and aged at 150 °C for 6 h.

Synthesis of Au NPs. Au NPs were synthesized by the method reported by Hiramatsu et al. with a small modification.[12a] Typically, 7 nm NPs were prepared by heating 0.4 g of $HAuCl_4 \cdot 3H_2O$, 20 mL of OA, and 40 mL of toluene at 80 °C overnight. Similarly, Au NPs with an average diameter of 10 nm were prepared by annealing a similar reaction mixture at 90 °C overnight.

Synthesis of Au/Ni NPs. A total of 30 mg of Au NPs dissolved in 5 mL of hexane, 30 mL of OA, and 4 mmol of nickel acetylacetonate, $Ni(acac)_2$, were mixed and kept at 100 °C for 2 h. Then the mixture was annealed at 170 °C for 2 h, resulting into black colloidal core/shell NPs.

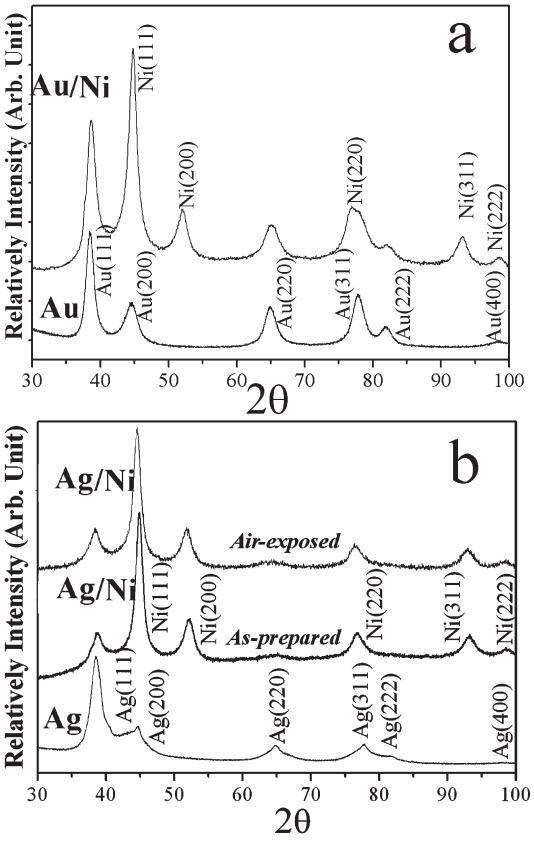

Figure 1. XRD patterns of (a) 7.0 nm Au NPs and 21.8 nm core/shell Au/Ni NPs with core size being 7.0 nm; (b) 12.0 nm Ag NPs, as-prepared and air-exposed 22.5 nm core/shell Ag/Ni NPs with core size being 12.0 nm.

Similarly, core/shell Ag/Ni NPs were synthesized with 40 mg of Ag NPs as starting templates.

Synthesis of Ni NPs. Ni NPs were synthesized by following the procedure reported by Chen et al.[12b] Typically, 1 mmol of $Ni(acac)_2$, 1 mmol of trioctylphosphine, 1 mmol of oleic acid, and 7 mL of OA were added into a flask. The 14. 2 nm Ni NPs were formed by heating the mixture at 245 °C for half an hour. Then 15.3, 18.3, and 23.5 nm Ni NPs were fabricated by adding another 1, 2, or 4 mmol of $Ni(acac)_2$, respectively, together with 20 mL of OA into reaction medium and annealing the mixture at 170 °C for 4 h.

Ligand Exchange. A total of 20 mg core/shell NPs and 0.5 g of imidazole were dissolved into 20 mL of toluene. Then the mixture was refluxed for 6 h under flowing N_2. After cooled to room temperature, the black powders were separated through centrifugation and dried in flowing N_2.

Characterization. Microstructure analysis of NPs was conducted using transmission electron microscopy (TEM; JEOL JEM 2010F) with an accelerating voltage of 200 kV. The crystal structures were analyzed by a X-ray diffraction (XRD) spectrometry (Bruker D8 Advance, U.S.A.) equipped with a Cu $K\alpha_1$ radiation source (λ = 0.15406 nm). For X-ray photoelectric spectroscopy (XPS) analysis, the samples were transferred to the sample chamber of a *Kratos* AXIS Ultra-DLD spectrometer and were irradiated with a monochromotized Al Kα X-ray source (1486.71 eV photons) at a vacuum of 10^{-9}–10^{-10} Torr. The depth profiling experiment was conducted with a high energy Ar^+ ions beam. All XPS spectra were referred by C 1s (284.5 eV) of hydrocarbon groups. The magnetic properties

(8) Li, D. S.; Komarneni, S. *J. Am. Ceram. Soc.* **2006**, *89*, 1510.
(9) (a) Ispas, C.; Andreescu, D.; Pahel, A.; Goia, D. V.; Andreescu, S.; Wallace, K. N. *Environ. Sci. Technol.* **2009**, *43*, 6349. (b) Martin, C. R.; Mitchell, D. T. *Anal. Chem.* **1998**, *70*, 322. (c) Lee, I. S.; Lee, N.; Park, J.; Kim, B. H.; Yi, Y. W.; Kim, T.; Kim, T. K.; Lee, I. H.; Paik, S. R.; Hyeon, T. *J. Am. Chem. Soc.* **2006**, *128*, 10658. (d) Lee, K. B.; Park, S.; Mirkin, C. A. *Angew. Chem., Int. Ed.* **2004**, *43*, 3048. (e) Hultgren, A.; Tanase, M.; Felton, E. G.; Bhadriraju, K.; Salem, A. K.; Chen, C. S.; Reich, D. H. *Biotechnol. Prog.* **2005**, *21*, 509. (f) Guo, D. D.; Wu, C. H.; Li, X. M.; Jiang, H.; Wang, X. M.; Chen, B. A. *J. Nanosci. Nanotechnol.* **2008**, *8*, 2301.
(10) (a) Ang, K. H.; Alexandron, I.; Mathur, N. D.; Amaratunga, G. A. J.; Hap, S. *Nanotechnology* **2004**, *15*, 520. (b) Johnston-Peck, A. C.; Wang, J. W.; Tracy, J. B. *ACS Nano* **2009**, *3*, 1077.
(11) Chen, M.; Feng, Y. G.; Wang, X.; Li, T. C.; Zhang, J. Y.; Qian, D. J. *Langmuir* **2007**, *23*, 5296.
(12) (a) Hiramatsu, H.; Osterloh, F. E. *Chem. Mater.* **2004**, *16*, 2509. (b) Chen, Y.; Peng, D. L.; Lin, D.; Luo, X. *Nanotechnology* **2007**, *18*, 505703.

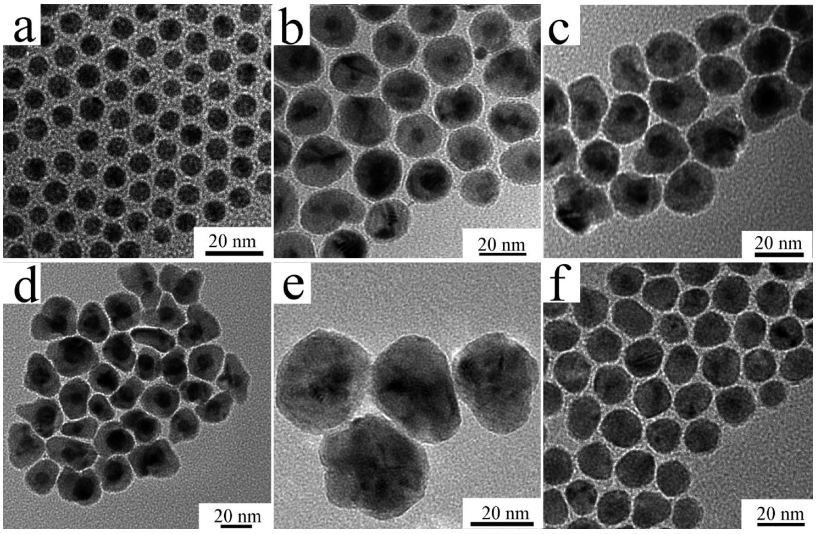

Figure 2. TEM image of (a) 7.0 nm Au NPs; (b−d) core/shell Au/Ni NPs with core size being 5.3 nm, 7.0 nm, and 9.9 nm; (e) 28.5 (±2.4) nm core/shell Ag/Ni NPs with core size being 12.0 nm; and (f) 15.3 (±1.4) nm Ni NPs.

were measured using a superconducting quantum interference device (SQUID; Quantum Design, U.S.A.).

Results and Discussion

The XRD patterns of as-prepared 21.8 (±2.1 nm) core/shell Au/Ni NPs with the core size being 7.0 (±0.7) nm and colloidal Au NPs are presented in Figure 1a. All diffraction peaks of Au NPs can be indexed to face-centered cubic (fcc) crystal structure.[13] The cell parameter of as-prepared Au NPs calculated by CELL software is 4.076 Å, which is very close to that ($a_0 = 4.078$ Å) of bulk gold crystal.[13] The XRD pattern of Au/Ni NPs indicates that the included Au cores exhibit the fcc crystal structure and have a unit cell parameter of 4.073 Å, which is also close to that of bulk gold.[13] The results reveal that the Au NPs were stable and were reminiscent of the original fcc structure. As to the shell component, five characteristic peaks ($2\theta = 44.83$, 52.06, 76.90, 93.09, and 98.2) for fcc Ni marked by their reflection indices (111), (200), (220), (311), and (222) were observed.[13] No diffraction peaks of Ni_2O_3, NiO, or $Ni(OH)_2$ were observed. The unit cell parameter of Ni shell is 3.528 Å and agrees well with that of bulk counterpart.[13] To check the generality of non-magnetic metal NPs, we also employed Ag NPs as the template. Our study indicated that Ag NPs could also be used as templates to synthesize core/shell NPs. In addition, we have checked the other kinds of M (Pd and Pt) NPs. Our study indicated that Pd and Pt NPs are not suitable for the application as core because they tend to alloy with Ni to form solid solution ($Pt_{1-x}Ni_x$ and $Pd_{1-x}Ni_x$) instead of core/shell NPs. Figure 1b shows the XRD patterns of Ag NPs and core/shell Ag/Ni NPs. Similar to these core/shell Au/Ni NPs, the shell of Ag/Ni is of pure fcc Ni, and the core of Ag/Ni NPs remained in Ag crystal structure with a lattice parameter of 4.083 Å.[13] To study the air stability, 22.5 (±2.3) nm Ag/Ni NPs with core size being 12.0 (±0.9) nm have been re-characterized after they had been stored on the XRD holder in air for one month. As shown in Figure 1b, the air-exposed sample exhibits a similar XRD pattern to that of the as-prepared Ag/Ni NPs, and no peaks of oxide species appear. The results reveal that Ni shell of core/shell NPs is relatively air stable.

Figure 2 shows typical TEM images of M NPs and as-prepared core/shell NPs. TEM analysis indicates that Au NPs synthesized by reducing $HAuCl_4$ with OA are of highly monodispersed size. As shown in Figure 2a, Au NPs formed at 80 °C overnight have an average diameter of 7.0 (±0.7) nm. Figure 2c shows a TEM image of Au/Ni NPs synthesized with 7.0 nm Au NPs as the template core. It is obvious that the 21.8 (±2.1) nm core/shell NPs possess a narrow size distribution and symmetrical shell. Our study also indicates that 5.3 nm and 9.9 nm Au NPs could also be employed to fabricate core/shell NPs by this procedure. In addition, our systemic study indicates that the shell thickness of core/shell particles with core size from 5 to 12 nm could be tuned from 5 nm to 10 nm by using this method, as shown in Figure 2b−d. As shown in Figure 2e, 28.5 (±2.4) nm core/shell Ag/Ni NPs formed with 12.0 nm Ag NPs also exhibit a relatively narrow size distribution.

Provided that the metallic Ni exposed to air will be inevitably oxidized to constant depth, the surface states of core/shell Au/Ni and Ni NPs were analyzed by XPS. Figure 3a shows the typical doublet of Ni $2p_{1/2}$ and $2p_{3/2}$ transitions for 21.8 nm Au/Ni NPs with core size being 7.0 nm. In the Ni $2p_{3/2}$ region, the sharp peak at binding energy of 851.8 eV (22 %) and peak at 855.4 eV (78 %) with broad shoulder could be assigned to metallic Ni and divalent nickel oxide species, respectively.[14] The atomic concentration was derived simply from integrated peak areas using the standard sensitivity factors. For the sake

(13) (a) Gold, Joint Committee on Powder Diffraction Standards (JCPDS), No. 04-0784, $a_0 = 4.078$ Å. (b) Nickel, JCPDS, No. 03-1043, $a_0 = 3.533$ Å. (c) Silver, JCPDS, No. 04-0783, $a_0 = 4.086$ Å.

(14) Wagner, C. D.; Riggs, W. M.; Davis, L. E.; Moulder, J. E. *Handbook of X-ray Photoelectron Spectroscopy*; Muilenberg, G. E., Ed.; Perkin-Elmer: Eden Prairie, MN, 1979.

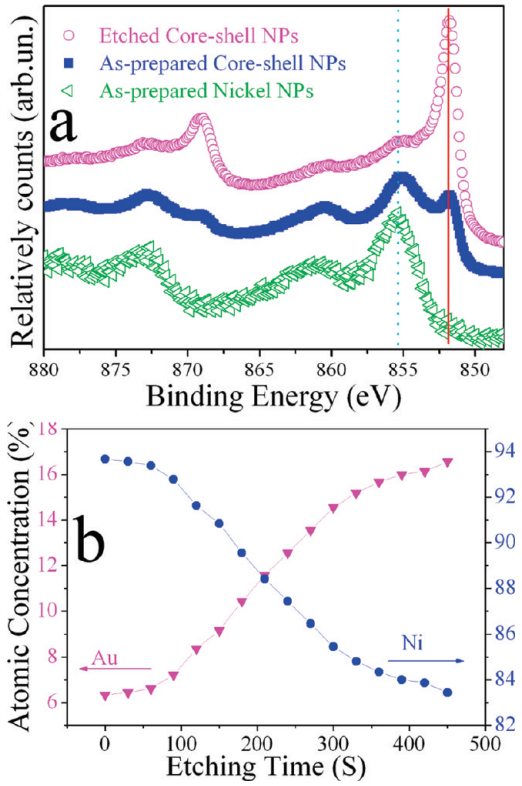

Figure 3. (a) XPS Ni 2p core level spectra of 21.8 nm core/shell Au/Ni NPs with core size being 7.0 nm and as-prepared 15.3 nm Ni NPs. (b) Relative concentration-depth profile of 21.8 nm core/shell Au/Ni NPs with core size being 7.0 nm.

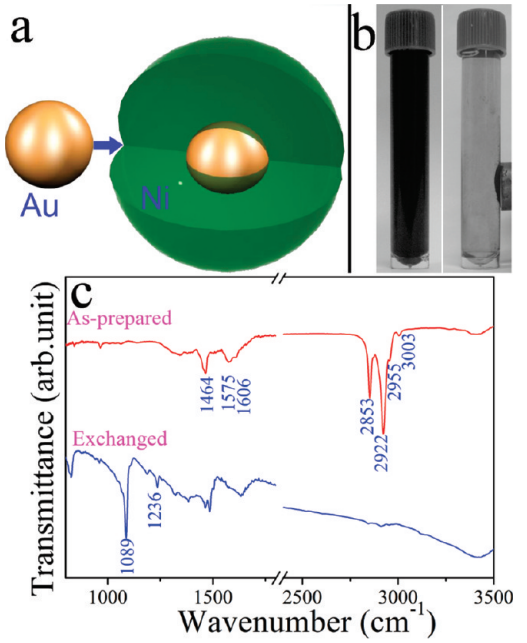

Figure 4. (a) Proposed formation mechanism of core/shell Au/Ni NPs. (b) Pictures indicate that 21.8 nm core/shell Au/Ni NPs with core size being 7.0 nm can be transferred to be water-soluble and re-separated by one permanent magnet. (c) FT-IR spectra of as-prepared and ligand exchanged 21.8 nm core/shell Au/Ni NPs.

of comparison, we also characterized 15.3 nm Ni NPs, and the Ni 2p region spectrum is also presented in Figure 3a. It is clear that there is only one peak with broad shoulder at binding energy of 855.4 eV. The lower intensity peak around 861 eV should be assigned to the typical satellite peak of $Ni(OH)_2$.[14] The nickel oxide species of the core/shell NPs decreased greatly (29 %) after the surface had been ion sputtered for 120 s. As for Ni NPs, it is obvious that only one peak with broad shoulder at binding energy of 855.4 eV was observed. Such a feature had often been observed in the Ni NPs system prepared in either an aqueous or an organic reaction system.[5e,15] It should be pointed out that our XRD and TEM studies indicate that there is no observable presence of nickel oxide or hydroxide in either M/Ni or Ni NPs. The XPS result indicates that a few atomic layers of divalent nickel species with disordered arrangement exist on the surface. The oxidized layer of bigger core/shell M/Ni NPs is thinner owing to fewer specific surface atoms and lower chemically active surface atoms.[5d] In other word, the bigger core/shell NPs exhibit a better anti-oxidation ability than smaller metallic Ni NPs because of fewer oxidized surface atoms, and some plausible reasons from the included M NPs. To verify the core/shell structure, we have conducted a depth profile measurement on the as-prepared 21.8 nm core/shell Au/Ni bimetallic NPs with core size being 7.0 nm. The analysis of the depth profile, as illustrated in Figure 3b, demonstrates clearly that Au contraction increases with increasing sputter time. On the contrary, the Ni concentration decreases with increasing sputter time. The behavior reveals that Ni and Au did not form a uniform solid solution. The results confirm that the NPs are of a typical core/shell structure.

The core/shell nanostructures should be formed by a typical template process, as illustrated in the Figure 4a. As reported previously, the nucleation of metallic Ni occurred at about 180 °C and was triggered by the dissociation of acetylacetone from the $Ni(acac)_2$ precursors with the elimination of water and carbon dioxide.[5d] The Ni clusters would tend to nucleate heterogeneously on the surface of Au NPs to reduce overall surface energy of the NP system at lower reaction temperature. Therefore, the Au/Ni NPs were formed after Ni atoms nucleated and grew on these M NPs.

Considering that NPs are generally applied in aqueous environments (such as magnetic separation and MRI), we conducted a ligand-exchange study in the hydrophobic NPs. To make the hydrophobic NPs water-soluble, we replaced the hydrophobic surfactants presented on the surface with imidazole molecules in toluene. As shown in Figure 4c, the stretching modes of as-prepared particles at 2853, 2922, 2955, and 3003 cm^{-1} are assigned to the well-known backbone of OA.[16a] After the ligand exchange process, the four modes of OA almost disappear. On the contrary, the stretching modes at 1236 cm^{-1} assigned to

(15) Couto, G. G.; Klein, J. J.; Schreiner, W. H.; Mosca, D. H.; de Oliveira, A. J. A.; Zarbin, A. J. G. *J. Colloid Interface Sci.* **2007**, *311*, 461.

(16) (a) Klokkenburg, M.; Hilhorst, J.; Erné, B. H. *Vib. Spectrosc.* **2007**, *43*, 243. (b) Masciocchi, N.; Bruni, S.; Cariati, E.; Cariati, F.; Galli, S.; Sironi, A. *Inorg. Chem.* **2001**, *40*, 5897.

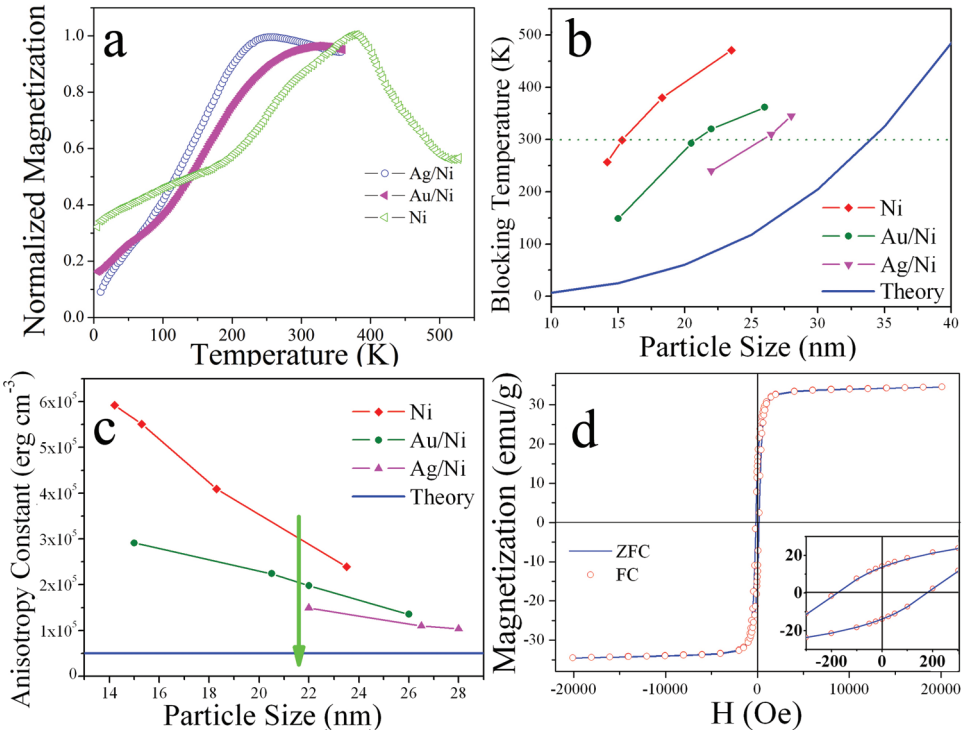

Figure 5. (a) Magnetization dependence of temperature measured under ZFC procedures with an applied field of 100 Oe for 21.8 nm core/shell Au/Ni, 22.5 nm core/shell Ag/Ni, and 18.3 nm Ni NPs. Diagrams of size dependence of blocking temperature (b) and size dependence effective anisotropy constant (c) for as-prepared Ni NPs, core/shell NPs, and theoretical values calculated by using Stoner-Wohlfarth models.[18] (d) $M-H$ loops of 21.8 nm core/shell Au/Ni NPs with core size being 7.0 nm measured at 10 K under ZFC and FC processes with an applied field of 2 Tesla; inset shows the low field detail of the cycles.

ring vibration and at 1089 cm^{-1} assigned to δ(C−H) of imidazole obviously appear.[16b] FT-IR analysis indicates that almost all hydrophilic molecules (OA) have been replaced by hydrophobic imidazole molecules.

The imidazole stabilized NPs could be re-dispersed easily into pure water by shake or ultrasonication, resulting in a clear dark dispersion (Figure 4b). Interestingly, the dispersed NPs could be separated by one permanent magnet within 3 min and be readily re-dispersed into water by shake or ultrasonication. In addition, the effects of pH value and concentration on stability of the core/shell NPs have been explored. Our study indicates that the stability of core/shell NPs in water decreases with increasing concentration, and they do not agglomerate significantly, which arises from the remanent magnetization, below a concentration about 0.15 mg/mL within half an hour. Such a behavior will enable them to settle onto the biomolecules enough before they agglomerate together. Furthermore, pH effect on the stability of water-soluble NPs has been checked. The NPs could be etched soon by chloric acid below a pH value of 5.0 and agglomerated immediately when the pH value was tuned to 12.0 by NaOH. The study indicates that the core/shell NPs are stable in the pH range of 6.5−10.5.

Magnetic properties were systematically studied using a SQUID magnetometer. Under an applied field of 100 Oe, zero-field-cooling (ZFC) and field-cooling (FC) procedures were employed to measure the temperature dependence of magnetization. Measurement indicates that FC magnetization of the NPs synthesized here decreases with increasing temperature. Figure 5a shows typical ZFC magnetization dependence of temperature curves of M/Ni NPs. Remarkably, the magnetization initially increases starting from 5 K with increasing temperature in the ZFC process. Then the magnetization reaches one maximum point, which is defined as the blocking temperature (T_B). It corresponds to the appearance of superparamagnetism. Eventually, the magnetization decreases slowly with increasing temperature above blocking temperature. Blocking temperatures of 21.8 nm Au/Ni NPs with core size being 7.0 nm and 22.5 nm Ag/Ni NPs with core size being 12 nm are 324 K and 240 K, respectively. Usually, size, shape, and morphology effects on magnetic properties were studied widely.[5d,17] To study the doping effect of non-magnetic M NPs on the magnetism of Ni NPs, we measured blocking temperatures of core/shell M/Ni with different core sizes and shell thicknesses. It should be noted that the M NPs used as template for core/shell NPs with different shell thicknesses were prepared in the same batch. As to core/shell NPs with size of around 22 nm, the blocking temperature decreases from 324 K to 240 K when the core size was enlarged from 7.0 to 9.9 nm. To investigate the effect of the non-magnetic core on the magnetism of Ni, temperature dependence magnetization of 18.3 (±1.5) nm Ni NPs is shown in Figure 5a. The 18.3 nm Ni has a blocking

(17) (a) Zhang, H. T.; Chen, X. H. *Nanotechnology* **2006**, *17*, 1384. (b) Zhang, H. T.; Chen, X. H. *Nanotechnology* **2005**, *16*, 2288. (c) Park, J.; An, K. J.; Hwang, Y. S.; Park, J. G.; Noh, H. J.; Kim, J. Y.; Park, J. H.; Hwang, N. M.; Hyeon, T. *Nat. Mater.* **2004**, *3*, 891. (d) Zhang, H. T.; Ding, J.; Chow, G. M. *Langmuir* **2008**, *24*, 375. (e) Zhang, H. T.; Chen, X. H. *J. Phys. Chem. B* **2006**, *110*, 9442.

temperature of above room temperature (378 K), which is higher than that of core/shell NPs with a bit larger size. The results indicate that these non-magnetic NPs really can reduce the effective magnetic anisotropy and, therefore, the blocking temperature of Ni NPs.

For comparison, we also have synthesized Ni NPs with different sizes in OA by a template procedure. As shown in Figure 2f, the Ni NPs also exhibit a narrow size distribution. Figure 5b presents the size dependence of blocking temperature of core/shell NPs and Ni NPs. As to metallic Ni and core/shell NPs, their blocking temperature increases with increasing particle size. Our study reveals that 18.3 (±1.5) nm and 23.5 (±2.4) nm Ni NPs exhibit blocking temperatures of 378 and 471 K, respectively. Both of them are much higher than that of core/shell NPs with similar size, as illustrated in Figure 5b. As to the particles with the same size, both metallic Ni and core/shell NPs have higher blocking temperature than the theoretical value calculated on the basis of Stoner−Wohlfarth models.[18] Interestingly, our results reveal that blocking temperature decreases with increasing core size, as marked by the arrow in Figure 5c. The results indicate that magnetic behavior of Ni NPs could be modulated expectably by the introduction of non-magnetic metallic NPs as dopant. The scheme indicates that those core/shell Au/Ni NPs (size < 21 nm) are superparamagnetic at 300 K. The T_B increases with increasing shell thickness as a result of size effect.[5c,17c]

As known, the correlation between T_B and volume of particles could be explained by the Stoner−Wohlfarth models.[18] The magnetic anisotropy of a particle is proportional to its volume: $T_B = KV/25k_b$, where K is the average magnetic anisotropy constant, and k_b and V represent the Boltzmann constant and volume of single NP, respectively.[19a] Generally, the main contribution to the magnetic anisotropy of magnetic NPs is magnetocrystalline, shape anisotropy and exchange anisotropy. Previous study indicated that the influence from shape anisotropy became prominent for smaller NPs (≤10 nm) with highly anisotropic shape.[19b,c] As illustrated in Figure 4a, the Ni shell can be considered as a crimped two-dimensional Ni nanosheet. This characteristic will enhance the shape anisotropy of the spherical core/shell NPs. On the other hand, the exchange anisotropy between the antiferromagnetic oxide layer and ferromagnetic Ni increased with increasing surface-to-volume atom ratio.[19c] Therefore, magntocrystalline anisotropy, shape anisotropy, and exchange anisotropy play the key role on the enhanced effective magnetic anisotropy for these core/shell NPs. For a spherical NP with a T_B of 298 K, if the K value of bulk Ni (5×10^4 erg cm^{-3}) is substituted in this equation, the deduced diameter of NP is 34 nm.[20a] For the sake of comparison, the effective magnetic anisotropy constants (the average for whole particles) were calculated by the Stoner−Wohlfarth equation and are depicted in Figure 5c. It is clear that all NPs have enhanced effective magnetic anisotropy constants compared to the theoretical predictions. The enhanced constants were plausibly induced by the antiferromagnetic oxide layer on the surface, size effect, and shape effect, which has been found in many other NP systems.[17c] The effective magnetic anisotropy constants decrease with increasing particle size, which further confirm that the enhanced constants are induced partially by size effect. Furthermore, the thin surface oxide/hydroxide layer should be considered owing to their larger magnetic anisotropy constants. Bulk NiO and $Ni(OH)_2$ show antiferromagnetism at low temperature and have magnetic anisotropy constants of 5.0×10^6 erg/cm^3 and 4.9×10^7 erg/cm^3, respectively.[20b,c] Therefore, the total magnetic anisotropy of Ni and core/shell NPs were enhanced inevitably by the strong exchange coupling interactions at the interface between metallic Ni and these oxide species, which exhibit larger magnetic anisotropy constants. Therefore, these Ni and M/Ni NPs exhibit enhanced magnetic anisotropy. The enhancement of overall anisotropy can push the blocking temperature to the high temperature side, which is not desirable for the applications of magnetic NPs.

Fortunately, our results indicate that the effective magnetic anisotropy could be reduced by including the non-magnetic NPs. Figure 5c illustrates the size dependence of overall effective magnetic anisotropy constants for core/shell NPs and single-component Ni NPs. It is clear that the effective magnetic anisotropy constant decreases with increasing total particle size. On the other hand, as highlighted by the arrow, the effective anisotropy constant decreases greatly with increasing included particle size. As to 22 nm core/shell NPs, the effective magnetic anisotropy constant ratio for core/shell NPS with the core sizes of 12 nm, 7 nm, and 0 nm is about 3:4:6. This characteristic indicates that the non-magnetic M NPs can reduce the magnetic anisotropy of Ni NPs, and the total magnetic anisotropy decreases with increasing included non-magnetic core size. The results indicate that blocking temperature of Ni nanostructures could be tuned rationally not only by modulating the shell thickness but also by adjusting the included non-magnetic core size. The illustration reveals that non-magnetic cores could effectively weaken the overall magnetic anisotropy of Ni nanostructures.

To understand the effect of non-magnetic core on the Ni nanostructures, we conducted magnetization dependence of magnetic field measurement at 300 K. As shown in Figure 6a, the as-prepared 21.8 nm core/shell NPs exhibit a saturated magnetization value of 30.3 emu/g and a superparamagnetic behavior at 300 K. In comparison, the $M-H$ loops of 14.2 nm and 23.5 nm Ni NPs were measured at 300 K and are shown in Figure 6. The coercivity field and saturation magnetization of the

(18) (a) Stoner, E. C.; Wohlfarth, E. P. *Trans. R. Soc.* **1948**, *A240*, 599. (b) Stoner, E. C.; Wohlfarth, E. P. *IEEE Trans. Magn.* **1991**, *27*, 3475. (c) Meiklejohn, W. H.; Bean, C. P. *Phys. Rev.* **1957**, *105*, 904.
(19) (a) Chen, Q.; Zhang, Z. J. *Appl. Phys. Lett.* **1998**, *73*, 3156. (b) Park, S. J.; Kim, S.; Lee, S.; Khim, Z. G.; Char, K.; Hyeon, T. *J. Am. Chem. Soc.* **2000**, *122*, 8581. (c) Roca, A. G.; Grady, P. K.; Serna, C. J. *Nanotechnology* **2006**, *17*, 2783.
(20) (a) Bala, T.; Bhame, S. D.; Joy, P. A.; Prasad, B. L. V.; Sastry, M. *J. Mater. Chem.* **2004**, *14*, 2941. (b) Kondo, H. *J. Phys. Soc. Jpn.* **1960**, *15*, 1970. (c) Ichiyanagi, Y.; Kondoh, H.; Yokoyama, T.; Okamoto, K.; Nagai, K.; Ohta, T. *Chem. Phys. Lett.* **2003**, *379*, 345.

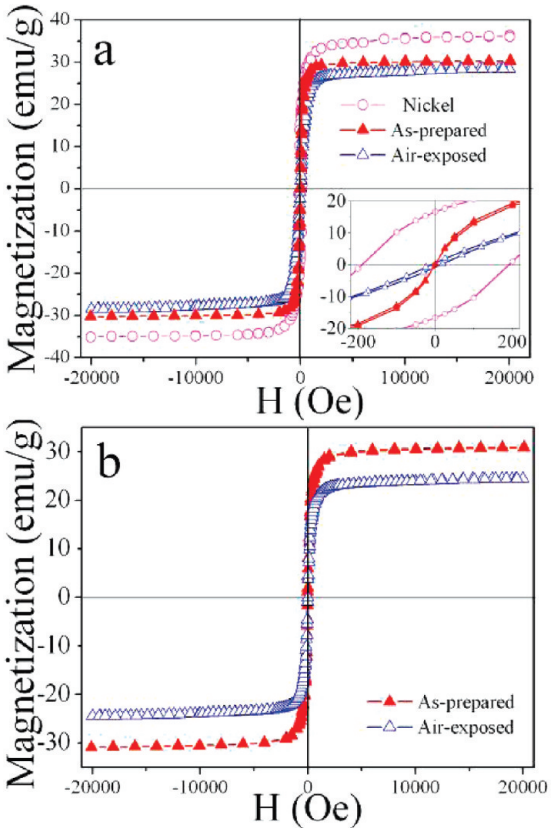

Figure 6. (a) $M-H$ loops of 23.5 nm Ni NPs, as-prepared and air-exposed 21.8 nm core/shell Au/Ni NPs with core size being 7.0 nm measured at 300 K; inset shows the low field details of the cycles. (b) $M-H$ loops of as-prepared and air-exposed 14.2 nm Ni NPs.

23.5 nm Ni at 300 K are 190 Oe and 36.4 emu/g. It implies that the non-magnetic NPs could reduce the overall saturation magnetization of core/shell NPs. On the other hand, 14.2 nm Ni NPs are superparamagnetic and exhibit a saturation magnetization of 30.9 emu/g. However, systemic study indicates that the saturation magnetization of metallic Ni NPs decreases greatly after they have been exposed in air for one month. As shown in Figure 6, saturation magnetization of 14.2 nm Ni NPs and 21.8 nm core/shell Au/Ni NPs decreased about 21% and 6%, respectively. This indicates that core/shell NPs are more air-stable. In other word, the bigger core/shell NPs exhibit improved anti-oxidation ability because of decreased surface-to-volume atomic ratio and the atoms are more passive in a low-curvature surface than those in a high-curvature surface. Therefore, the oxide layer of core/shell NPs is thinner, and the overall anisotropy is more close to that expected for pure bulk Ni.

The hysteresis loops of the 21.8 nm Au/Ni NPs were measured at 10 K, too. As shown in Figure 5d, the sample exhibits a saturated magnetization of 34.6 emu/g and coercivity of 190 Oe. The results indicate that the sample is ferromagnetic at low temperature. The saturated magnetization is far lower than the magnetization value (57.6 emu/g) for bulk Ni. According to the domain theory, Ni has a critical diameter of 21.2 nm.[22] It is well known that the thermal fluctuations will significantly reduce the total magnetic moment at a given field when a magnetic NP's energy becomes comparable to the thermal energy ($25k_bT$).[23] In addition, the disordered structure at interfaces and surfaces provides less magnetic moment per unit mass than that in ferromagnetic core regions, which also leads to a decrease in the saturated magnetization.[24] Furthermore, the non-magnetic core will inevitably reduce the long range magnetic ordering of Ni. Therefore, the saturation magnetization of core/shell NPs is lower than that of the corresponding bulk because of non-magnetic core and magnetically inactive layer.[5d,21]

The field cooling $M-H$ loop, which cooled from 320 K under a magnetic field of 2 Tesla, for 21.8 nm core/shell Au/Ni NPs with core size being 7.0 nm, was conducted to explore the affection of the atomic layers of oxide/hydroxide species on the magnetic properties. As highlighted in the inset of Figure 5d, the $M-H$ loop measured under the FC procedure is almost identical to that measured under the ZFC procedure. The results strongly suggest that the core/shell NPs are relatively air-stable, and the layer of oxide/hydroxide species on the surface is so thin that it is unable to support the interfacial pinning orientation necessary for an obvious exchange shift effect.[10b] Such a behavior further proves that the exchange couple on the interface between the oxide layer and elemental Ni is relatively small in the bigger core/shell NPs.

Conclusion

In summary, we demonstrate the design and fabrication of bimetallic nanostructures with non-magnetic cores and ferromagnetic shell though a simple template route. The magnetic properties of core/shell NPs could be controlled by tuning the core size and the shell thickness. Temperature dependence of the magnetization study indicates that the blocking temperature increased with increasing shell thickness and decreasing core size. Systematic study indicates that the effective magnetic anisotropy of core/shell NPs and Ni NPs increases with decreasing particle size and decreases with increasing wrapped core size. XRD, XPS, and SQUID studies suggest that the core/shell NPs are more stable in air compared to the metallic Ni NPs. Our study indicates that the core-shell NPs are relatively stable in the pH range of 6.5−10.5. These superparamagnetic larger NPs are promising candidates for biomarker, optoelectronics, and magnetic biomolecule separation. Our study elucidates a set of empirical guidelines for the rational design and fabrication of magnetic nanostructures with controllable expected magnetic properties by doping methodology, which can be extended to the other kinds of nanomaterials with the progress of nanomaterial synthetic methodology and understanding the fundamental properties of nanomaterials.

(21) Gong, W.; Li, H.; Zhao, Z.; Chen, J. *J. Appl. Phys.* **1991**, *69*, 5119.
(22) Shafi, K.V. P. M.; Gedanken, A.; Prozorov, R.; Balogh, J. *Chem. Mater.* **1998**, *10*, 3445.
(23) Hwang, J. H.; Dravid, V. P.; Teng, M. H.; Host, J. J.; Elliott, B. R.; Johnson, D. L.; Mason, T. O. *J. Mater. Res.* **1997**, *12*, 1076.
(24) Tamura, K.; Endo, H. *Phys. Lett.* **1969**, *29A*, 52.